Electronic Supplementary Information

Efficient Electrocatalytic Carbon Dioxide Reduction with Tetraphenylethylene and Porphyrin-Based Covalent Organic Frameworks

Lei Gong, Ying Gao, Yinhai Wang, Baotong Chen, Baoqiu Yu, Wenbo Liu, Bin Han, Chenxiang Lin, Yongzhong Bian, Dongdong Qi and Jianzhuang Jiang

Beijing Key Laboratory for Science and Application of Functional Molecular and Crystalline Materials, Department of Chemistry, School of Chemistry and Biological Engineering, University of Science and Technology Beijing, Beijing 100083, China

Daxing Research Institute, and Beijing Advanced Innovation Center for Materials Genome Engineering, University of Science and Technology Beijing, Beijing 100083, China

Guangxi Key Laboratory of Natural Polymer Chemistry and Physics, Nanning Normal University, Nanning 530001, China

Contents

EXPERIMENTAL SECTION

Materials

$CoPor(CHO)_4$ were synthesized following the published procedure.[1] All other regents were commercially available and used as received.

Characterization

NMR spectra were recorded on a Bruker DPX 400 spectrometer (^1H: 400 MHz) in D_2O. Powder X-ray diffraction (PXRD) was collected at room temperature on a PANalytical Empyrean series 3 diffractometer equipped with Cu K_α radiation. FT-IR spectra were recorded as KBr pellets using a Bruker Tensor 37 spectrometer with 2 cm^{-1} resolution. X-ray photoelectron spectroscopy (XPS) data were recorded on a Thermo Scientific K-Alpha system. Al K_α X-ray (6 mA / 12 KV) was utilized as the irradiation source. All XPS measurements were performed in the CAE mode with the reference of C 1s (284.8 eV). The nitrogen adsorption and desorption isotherms were measured at 77 K and the CO_2 adsorption and desorption isotherms were measured at 298 K using a Micromeritics ASAP 2020 PLUS HD88 system. The samples were degassed at 90°C for 4 hours before the measurements. The thermogravimetric analysis (TGA) was performed on a Rigaku TG-DTA8122 instrument over the temperature range from 30 to 800°C under nitrogen atmosphere with a heating rate of 10°C/min. The metal contents of TPE-CoPor-COF and TPTPE-CoPor-COF were determined by inductively coupled plasma (ICP) analysis with an Aglient 5110 ICP-OES instrument.

Energy dispersive spectroscopy (EDS) mapping images were collected by transmission electron microscopy (JEM-2100F) at an operation voltage of 200 kV. Scanning electron microscopy (SEM) images were obtained on a HITACHI SU8010 microscope. UV-vis-NIR diffuse reflectance spectra (DRS) were recorded on a Shimadzu UV-2600 UV-vis-NIR spectrophotometer with $BaSO_4$ as the reference.

Synthesis of TPE-CoPor-COF

$CoPor(CHO)_4$ (18.8 mg, 0.024 mmol), $TPE(NH_2)_4$ (9.4 mg, 0.024 mmol), *n*-butanol (0.36 mL), *o*-dichlorobenzene (1.44 mL), and 6 M aqueous acetic acid (0.18 mL) were mixed in a Pyrex tube (9 × 6 mm, o.d. × i.d.). After sonication for 10 min, the Pyrex tube was rapidly frozen in a liquid nitrogen bath and degassed. After the above process was repeated three times, the tube was sealed with alcohol torch. After the Pyrex tube were warmed to room temperature, the tube was placed in an oven at 120℃ for 72 h. The obtained COFs was placed in a Soxhlet extractor and washed with tetrahydrofuran (24 h) and chloroform (24 h) in turn. Finally, the product was dried under vacuum at 70°C for 12 h to provide TPE-CoPor-COF as purple powder (19.7 mg, ~70% yield).

Synthesis of TPTPE-CoPor-COF

TPTPE-CoPor-COF (21.7 mg, ~61% yield) was synthesized following the similar procedure for TPE-CoPor-COF, except that $TPE(NH_2)_4$ was replaced with $TPTPE(NH_2)_4$.

Electrochemical measurements.

All electrocatalysis tests were conducted at room temperature in a standard three-electrode configuration using H-type cell on an electrochemical workstation (chi760E). In the H-type cell, two compartments equipped with 0.5 M $KHCO_3$ aqueous solution were separated by an anion exchange membrane (Nafion-117). Ag/AgCl electrode and Pt foil were served as the reference and counter electrodes, respectively. A catalyst-modified carbon fiber paper electrode was used as the work electrode.

COFs or CoPor(CHO)$_4$/TPE(NH$_2$)$_4$/TPTPE(NH$_2$)$_4$ (5 mg), Vulcan XC-72R carbon black (5 mg), ethanol (965 μL) and Nafion perfluorinated resin solution (35 μL, 10 wt. % in H_2O) were mixed in a vial. Homogeneous pastes were formed after sonication for 60 min. To make sure that loading density of electrode materials was 1 mg cm^{-2}, 100 μL paste was dropped evenly onto a piece of carbon fiber paper (1 cm × 1 cm). The catalyst-modified carbon fiber paper electrode was placed in dark for 12 h. Before each electrochemical test, the electrolyte solution was saturated with Ar or CO_2 for 30 min. Linear sweep voltammetry (LSV) polarization curves were measured from 0 to −1.63 V *vs*. Ag/AgCl with a scan rate of 10 mV s^{-1}. On account of the following equation: E (*vs*. RHE) = E (*vs*. Ag/AgCl) + 0.197 V + 0.059 × pH, the results of electrocatalysis in this work were presented *vs*. RHE. Besides, no *iR* compensation was carried out for all LSV polarization curves.

EIS spectroscopies were measured under an AC voltage of −1.5 V vs Ag/AgCl with 5 mV amplitude in a frequency range from 1000 kHz to 100 mHz. Cyclic voltammograms (CV) tests were conducted to obtain C_{dl} under the potential window from 0.29 to 0.19 V *vs*. RHE with various scan rates from 10 to 100 mV s^{-1} to estimate

the ECSA.

Structure modeling

The unit cells of the models were refined with the experimental PXRD data of TPE-CoPor-COF and TPTPE-CoPor-COF by using the Le Bail refinement. The cell parameters and the refined PXRD patterns were obtained until the values of R_{wp} and R_p converged.

DFT calculation methods

Density functional theory (DFT) calculations were performed by PBE0-D3 method with Becke-Johnson damping.[2,3] A mixed basis set, including 6-31G(d) for C/H/N/O and SDD for Co, was utilized to optimize the structures and calculate the Gibbs free energies using Gaussian 09 program (version D.01).[4-8] Besides, the solvation model based on density (SMD) was used to simulate the aqueous environment.[9]

The electrocatalytic mechanisms were studied based on Nøskov's computational hydrogen electrode model.[10,11] In this technique, zero voltage was defined based on the potential energy (μ) of components involved in the reversible hydrogen electrode at all pH, T and p, therefore, $\mu(H^+) + \mu(e^-) = \frac{1}{2}\mu(H_2)$ at a potential of 0 V. The pathways adopted for CO_2 reduction to CO in this work are listed below (* represents the active site):

$$* + CO_2 + H^+ + e^- \rightarrow *COOH$$

$$*COOH + H^+ + e^- \rightarrow *CO + H_2O$$

$*CO \rightarrow * + CO$

In addition, the pathway adopted for hydrogen evolution reaction (HER) in this work is shown as below:

$* + H^+ + e^- \rightarrow *H$

Calculation of Faradaic Efficiency

The Faradaic efficiencies (FEs) for CO production at each applied potential were calculated based on the following equation:

$$FE = \frac{j_{CO}}{j_{total}} = \frac{\nu_{CO} \times N \times F}{j_{total}}$$

j_{CO}: partial current density for CO production; j_{total}: total current density; ν_{CO}: the production rate of CO; N: the number of transferred electrons (2 for CO); F: Faradaic constant, 96485 C mol^{-1}.

Calculation of Turnover Frequency (TOF, s^{-1})

The TOF for CO was calculated based on the following equation:

$$TOF = \frac{j_{total} \times FE_{CO} / NF}{\omega m_{cat} / M}$$

j_{total}: total current density; FE_{CO}: Faradaic efficiency for CO production (%); N: the number of electrons (2 for CO); F: Faradaic constant, 96485 C mol^{-1}; ω: the metal content of Co; m_{cat}: the catalyst mass in the electrode; M: the atomic mass of Co.

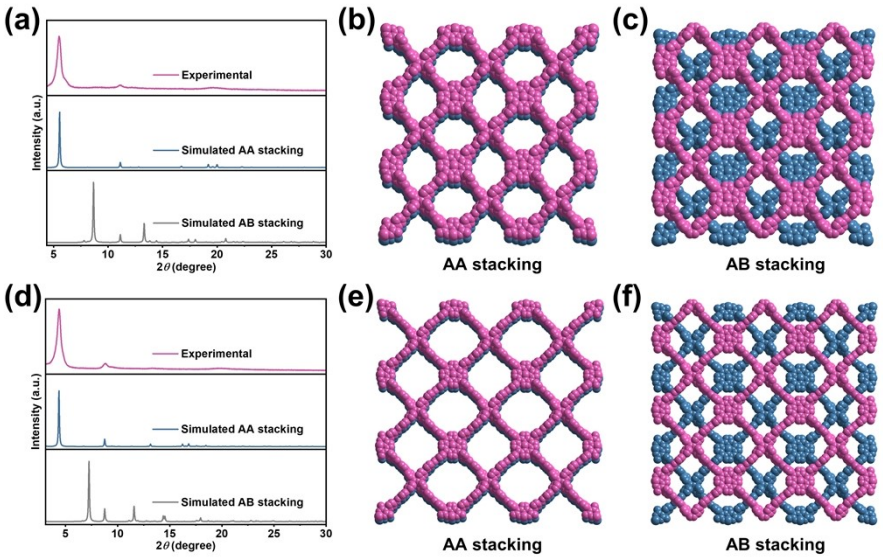

Fig. S1. Simulated PXRD patterns (a), AA stacking model (b) and AB stacking model (c) of TPE-CoPor-COF; Simulated PXRD patterns (d), AA stacking model (e) and AB stacking model (f) of TPTPE-CoPor-COF.

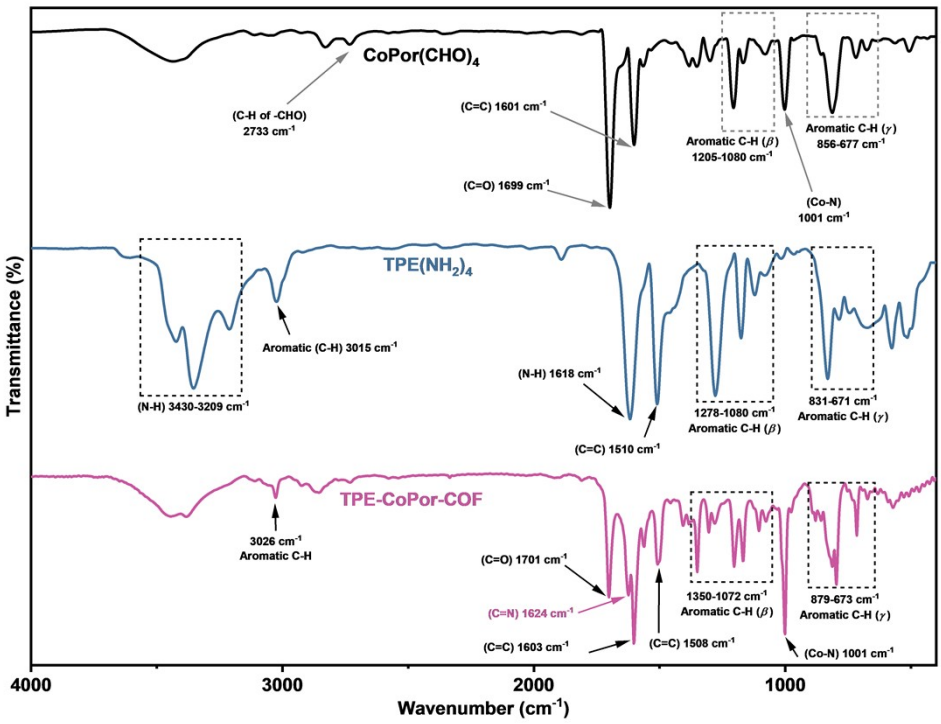

Fig. S2. FT-IR spectra of TPE-CoPor-COF.

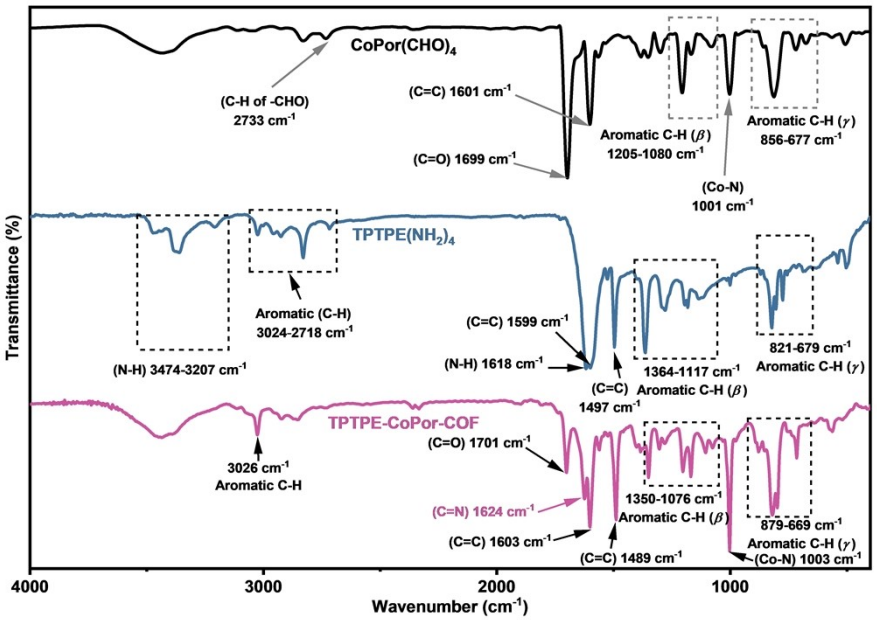

Fig. S3. FT-IR spectra of TPTPE-CoPor-COF.

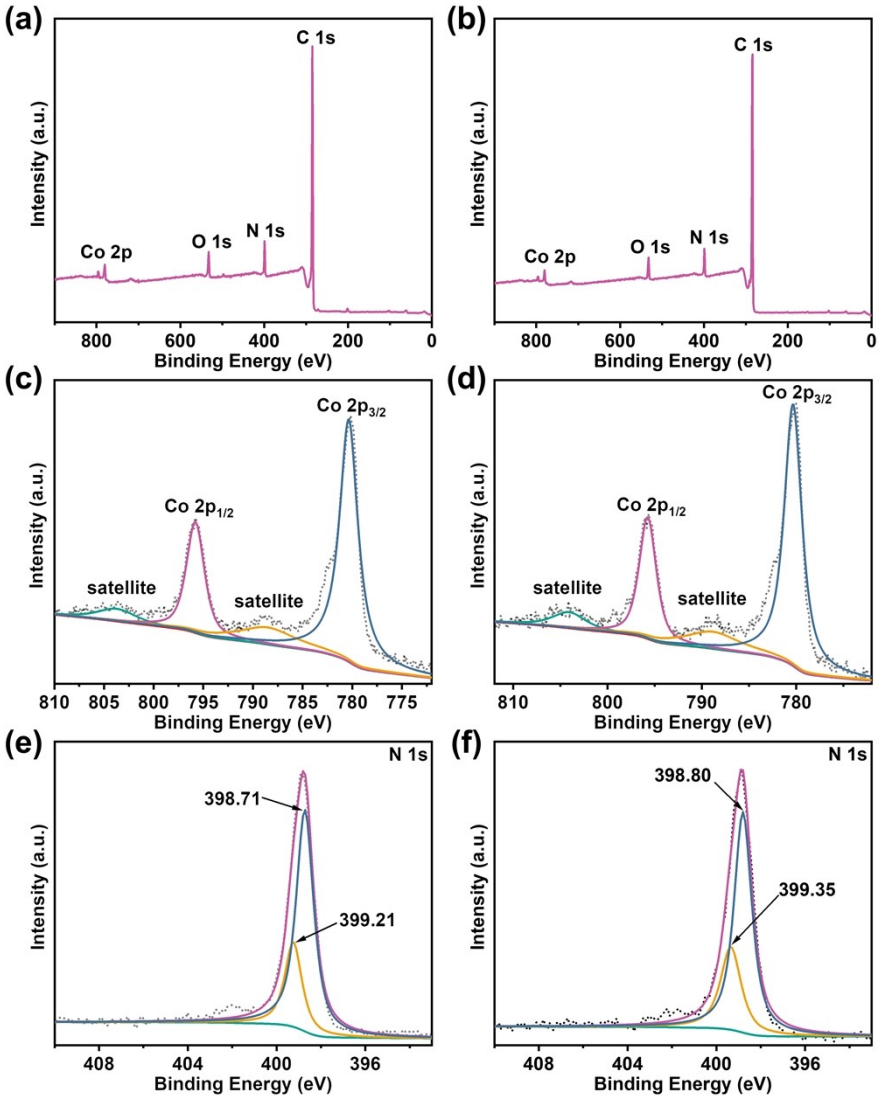

Fig. S4. Total XPS spectra of TPE-CoPor-COF (a), high-resolution scan of Co 2p (c) and high-resolution scan of N 1s (e) for TPE-CoPor-COF; Total XPS spectrum of TPTPE-CoPor-COF (b), High-resolution scan of Co 2p (d) and High-resolution scan of N 1s (f) for TPTPE-CoPor-COF.

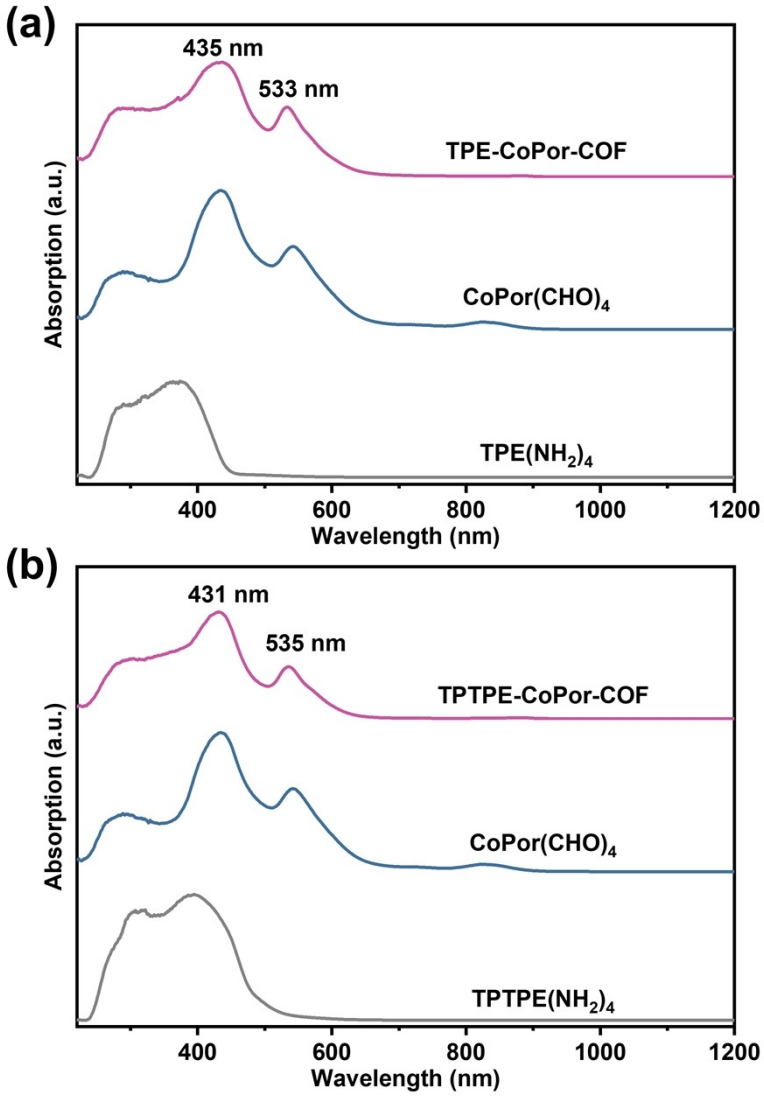

Fig. S5. The solid state UV-vis-NIR diffuse reflectance spectra (DRS) of (a) TPE-CoPor-COF and (b) TPTPE-CoPor-COF.

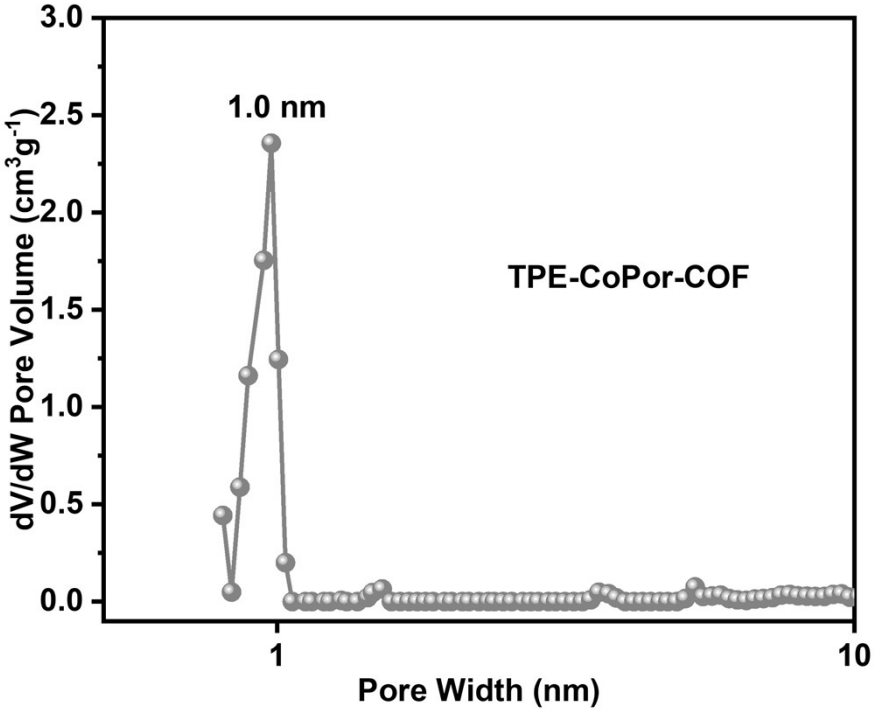

Fig. S6. Pore size distribution of TPE-CoPor-COF.

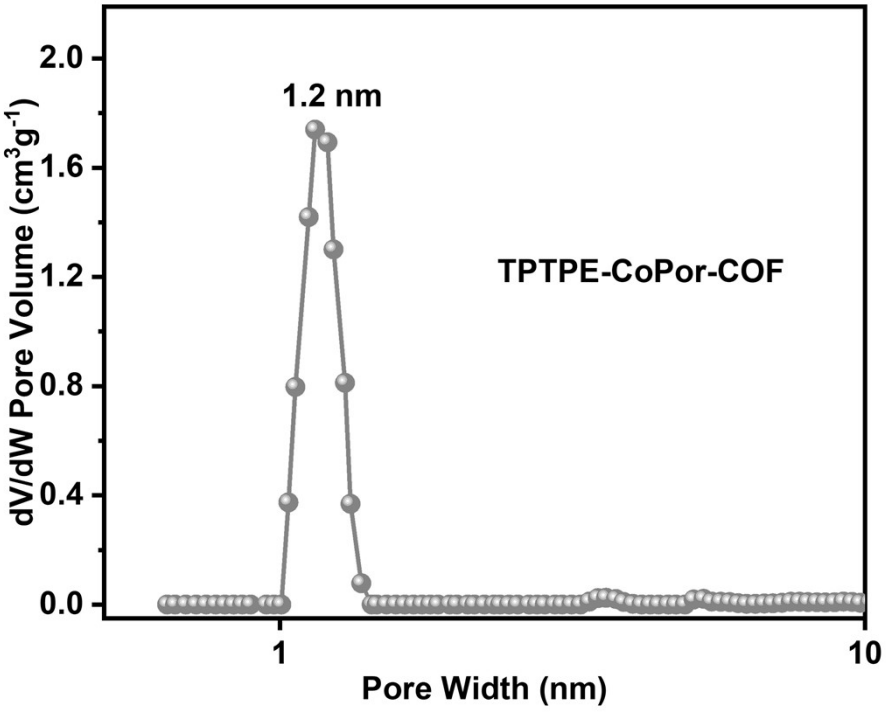

Fig. S7. Pore size distribution of TPTPE-CoPor-COF.

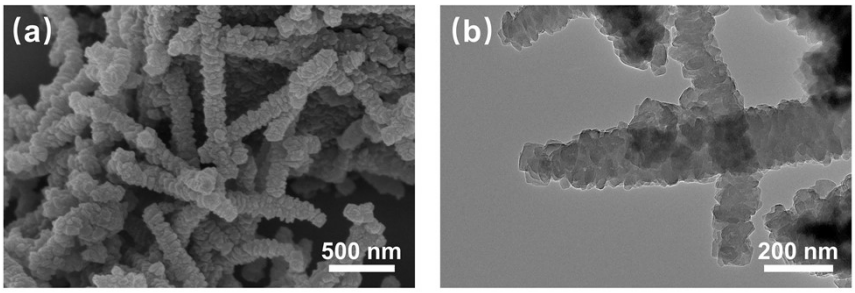

Fig. S8. (a) SEM and (b) TEM images of TPTPE-CoPor-COF.

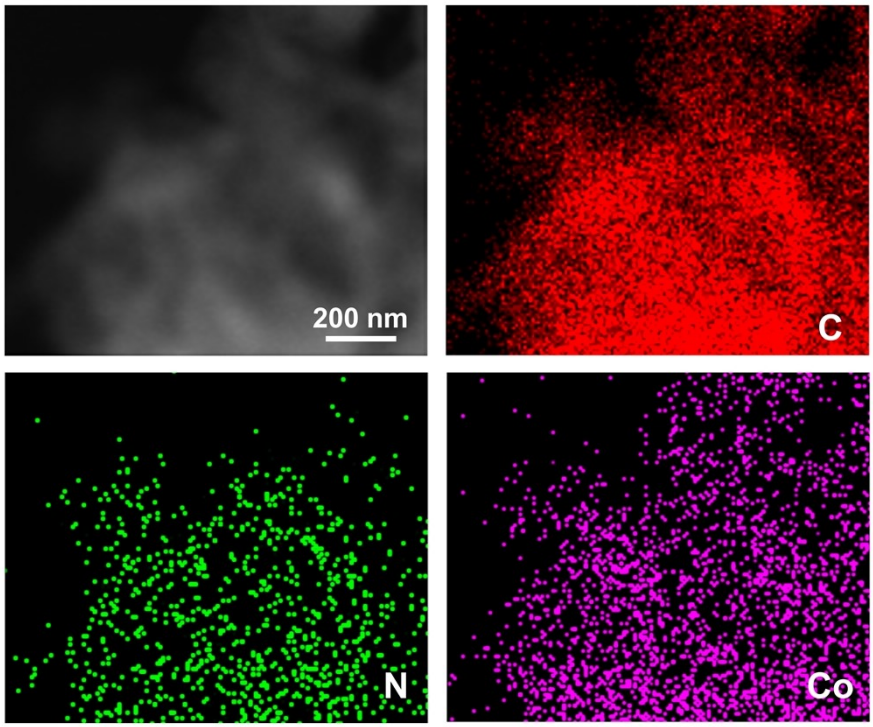

Fig. S9. Energy-dispersive spectroscopy (EDS) mappings of TPTPE-CoPor-COF.

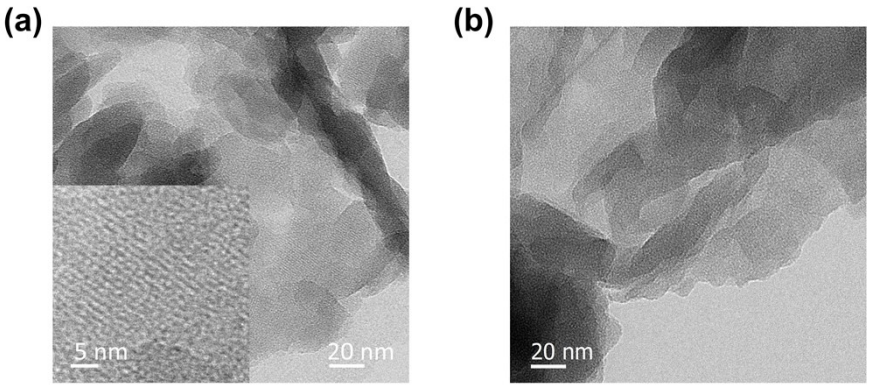

Fig. S10. HRTEM images of (a) TPE-CoPor-COF and (b) TPTPE-CoPor-COF.

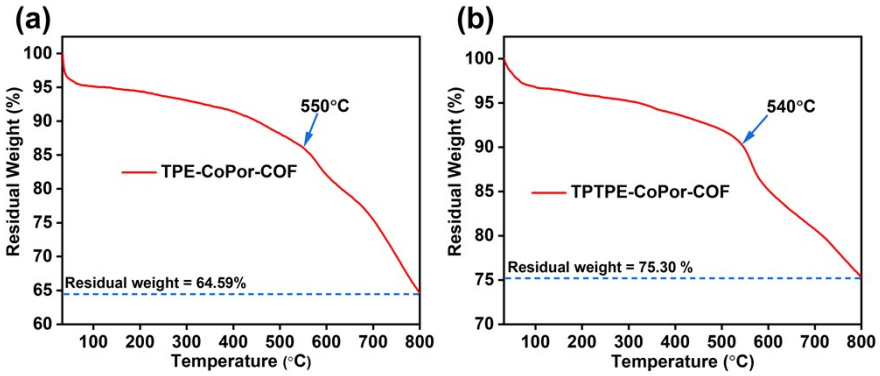

Fig. S11. Thermal gravimetric analysis of TPE-CoPor-COF and TPTPE-CoPor-COF, with a constant heating rate of 10°C min^{-1} from room temperature to 800°C under N_2 atmosphere.

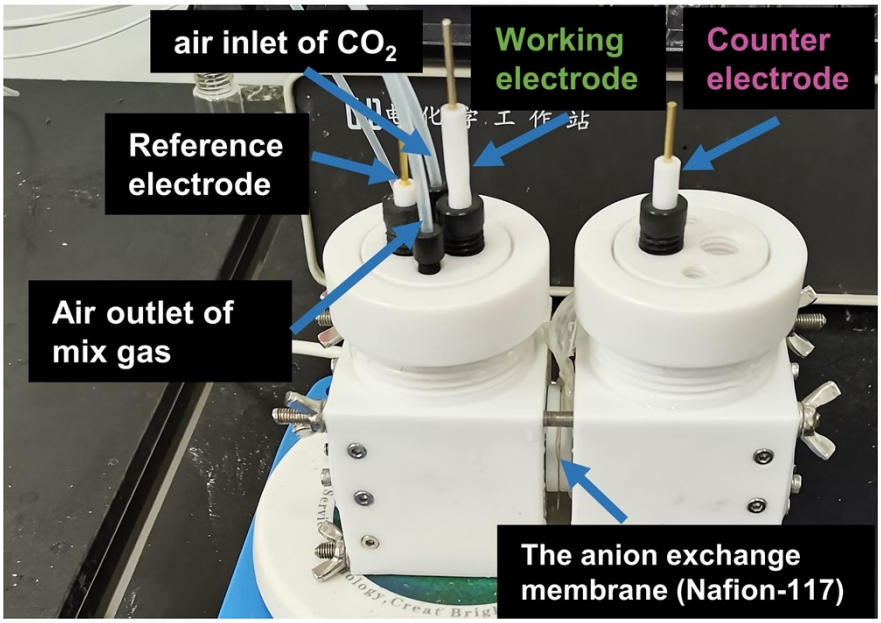

Fig. S12. Typical three-electrode H-type cell setup for electrochemical CO_2RR measurements.

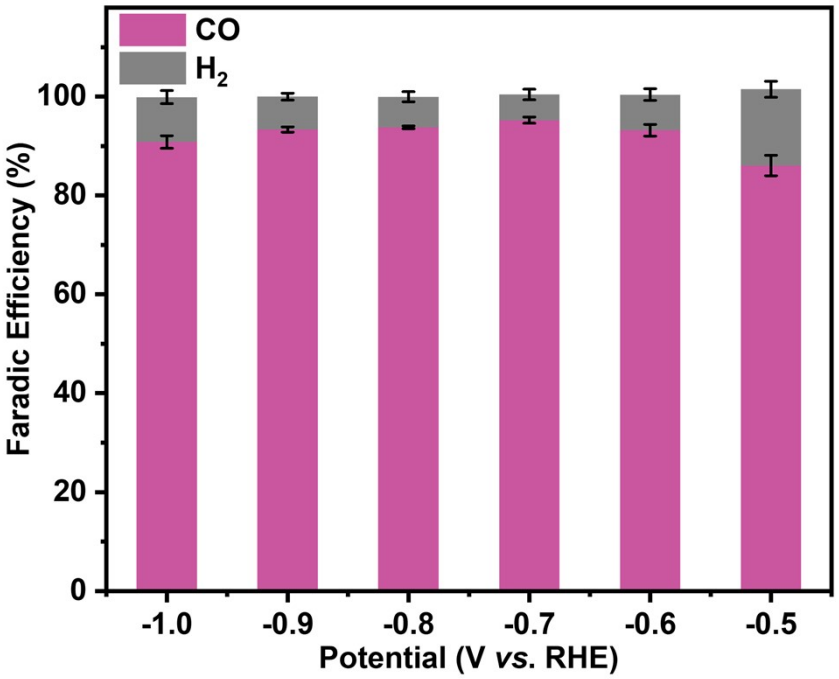

Fig. S13. FE_{CO} and FE_{H_2} of TPE-CoPor-COF at different applied potentials in CO_2 saturated 0.5 M $KHCO_3$ aqueous solution.

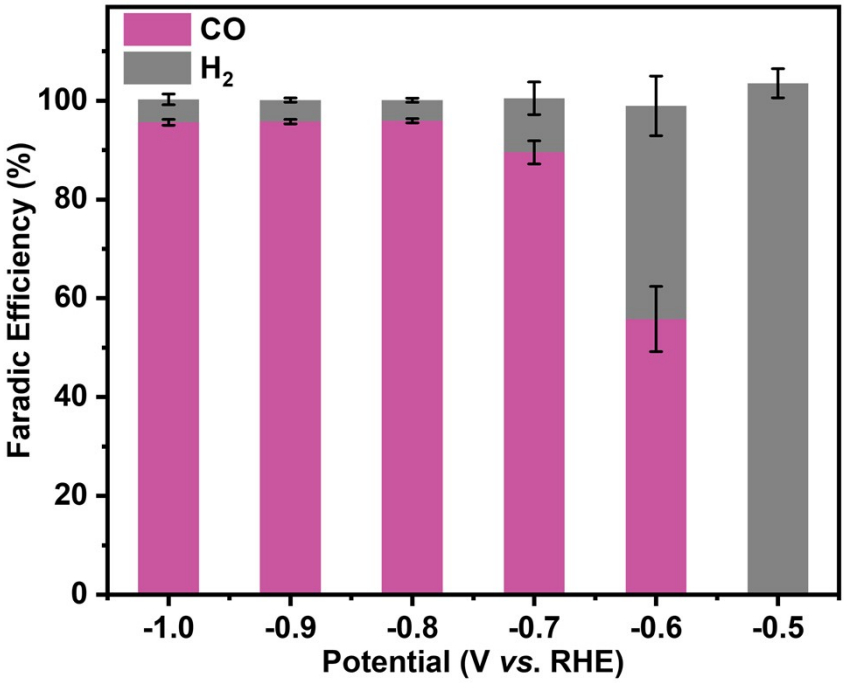

Fig. S14. FE_{CO} and FE_{H_2} of TPTPE-CoPor-COF at different applied potentials in CO_2 saturated 0.5 M $KHCO_3$ aqueous solution.

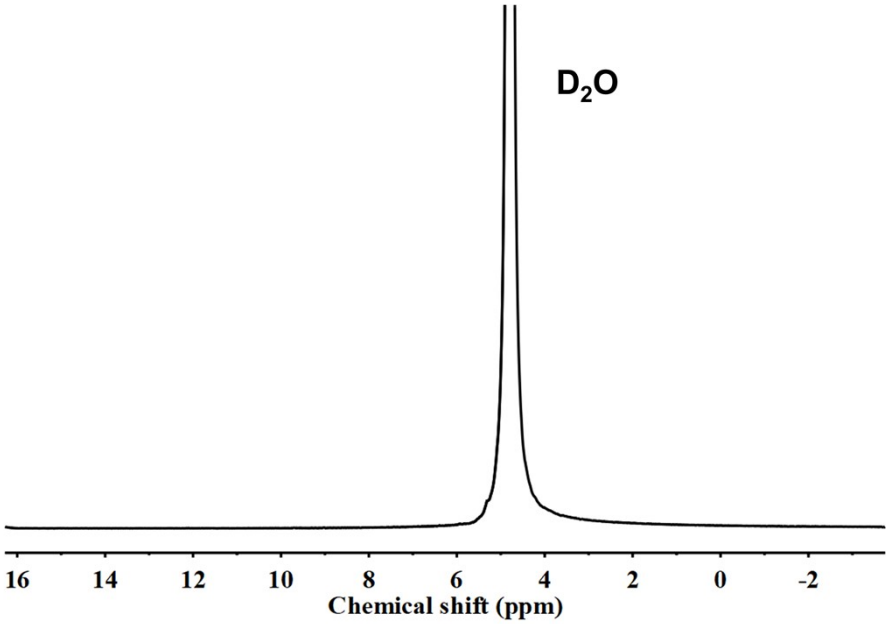

Fig. S15. ^{1}H NMR spectrum of the electrolyte for TPE-CoPor-COF after continuous CO_2RR tests (-0.50 to -1.0 V *vs*. RHE) in D_2O.

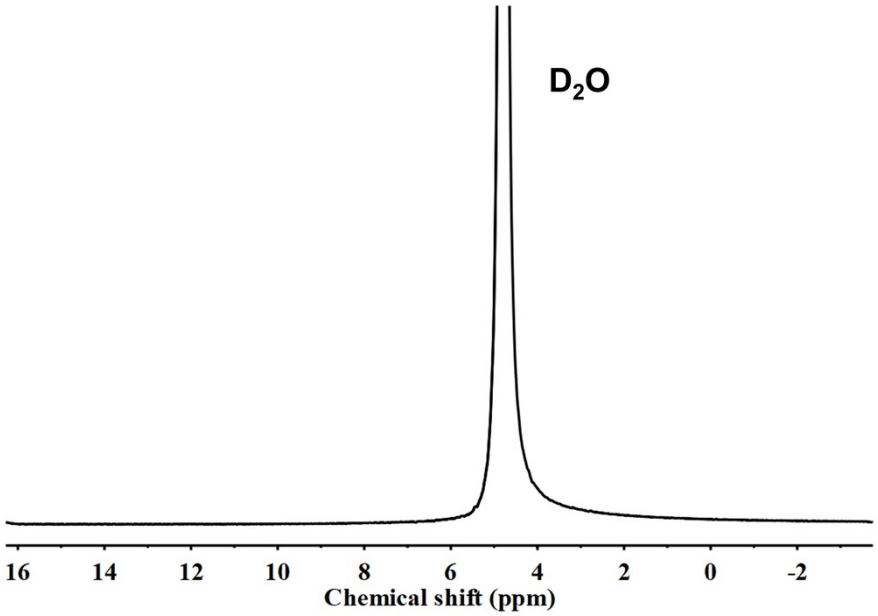

Fig. S16. ^{1}H NMR spectrum of the electrolyte for TPTPE-CoPor-COF after continuous CO_2RR tests (-0.50 to -1.0 V *vs*. RHE) in D_2O.

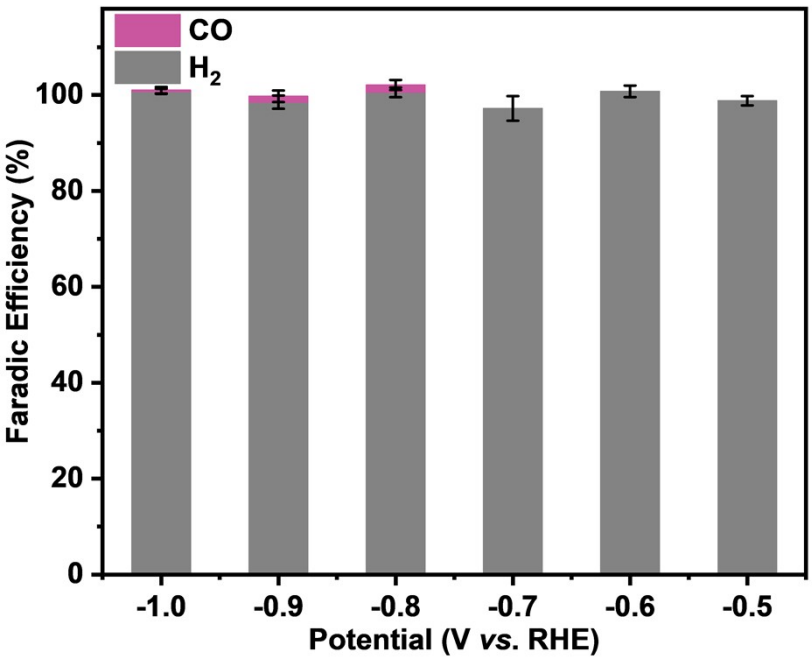

Fig. S17. FE_{CO} and FE_{H_2} of TPE-CoPor-COF at different applied potentials in Ar saturated 0.5 M $KHCO_3$ aqueous solution.

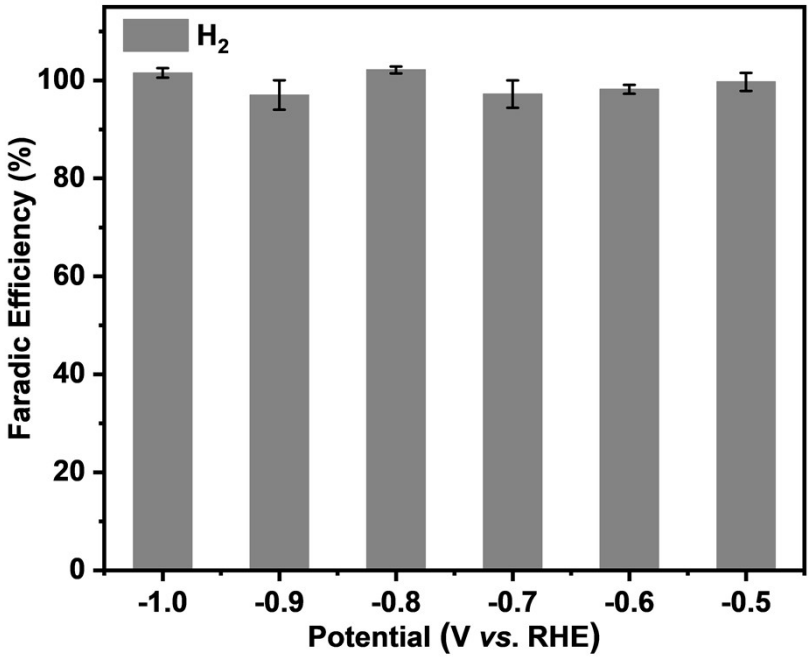

Fig. S18. FE_{CO} and FE_{H_2} of TPTPE-CoPor-COF at different applied potentials in Ar saturated 0.5 M $KHCO_3$ aqueous solution.

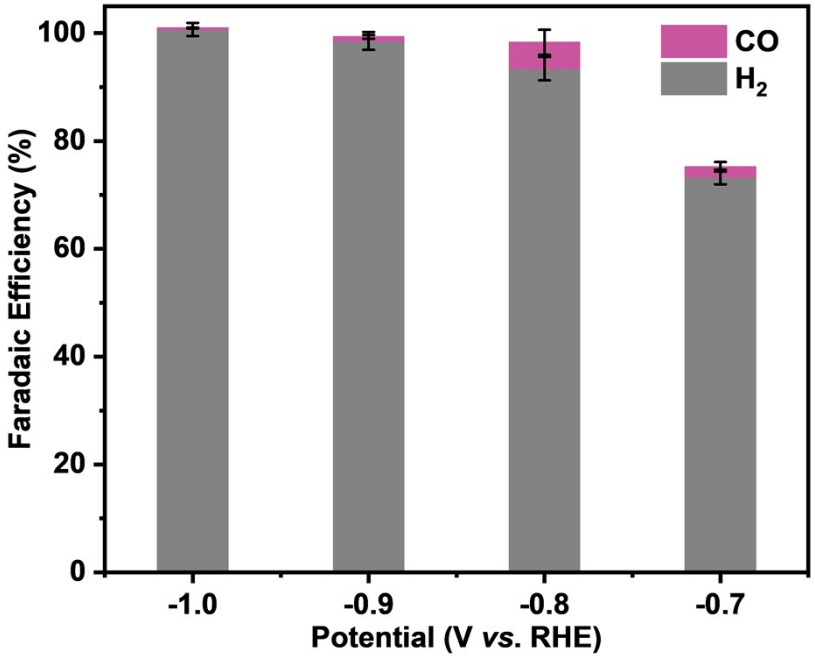

Fig. S19. FE_{CO} and FE_{H_2} of the carbon cloth with Vulcan XC-72R carbon black and Nafion at different applied potentials in CO_2 saturated 0.5 M $KHCO_3$ aqueous solution.

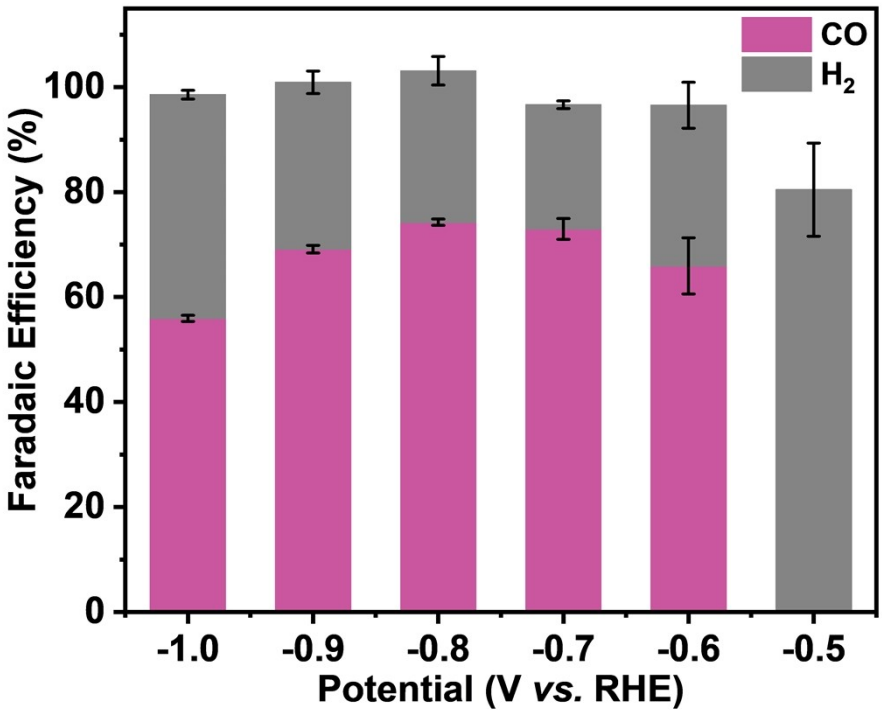

Fig. S20. FE_{CO} and FE_{H_2} of $CoPor(CHO)_4$ at different applied potentials in CO_2 saturated 0.5 M $KHCO_3$ aqueous solution.

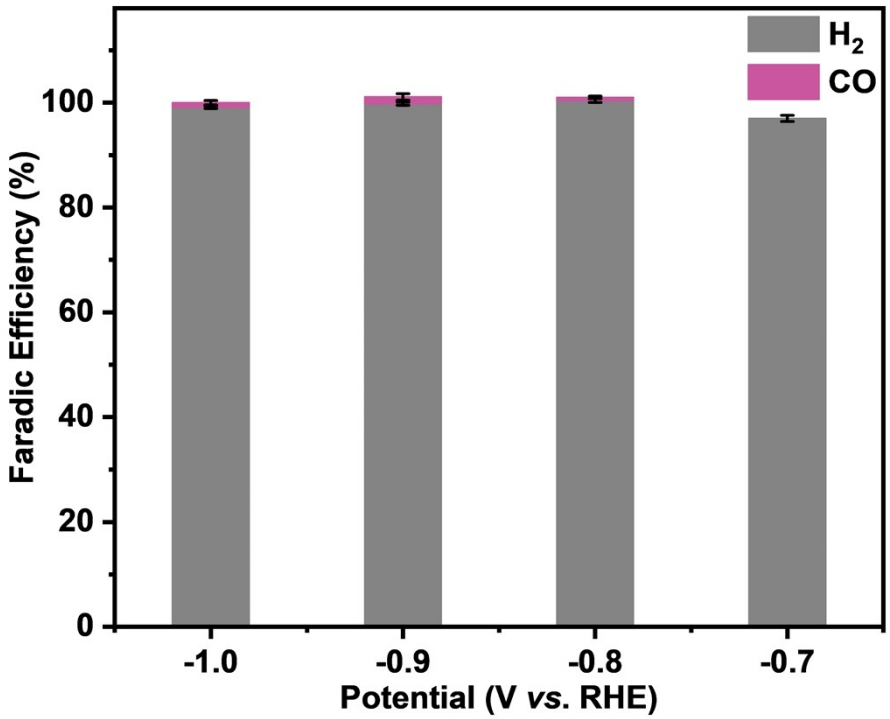

Fig. S21. FE_{CO} and FE_{H_2} of $TPE(NH_2)_4$ at different applied potentials in CO_2 saturated 0.5 M $KHCO_3$ aqueous solution.

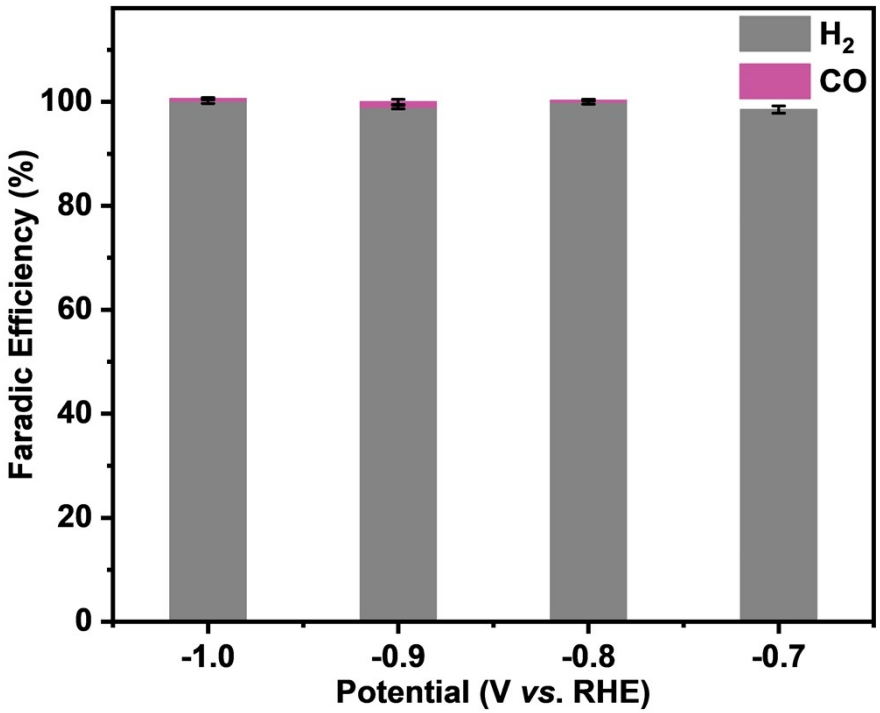

Fig. S22. FE_{CO} and FE_{H_2} of $TPTPE(NH_2)_4$ at different applied potentials in CO_2 saturated 0.5 M $KHCO_3$ aqueous solution.

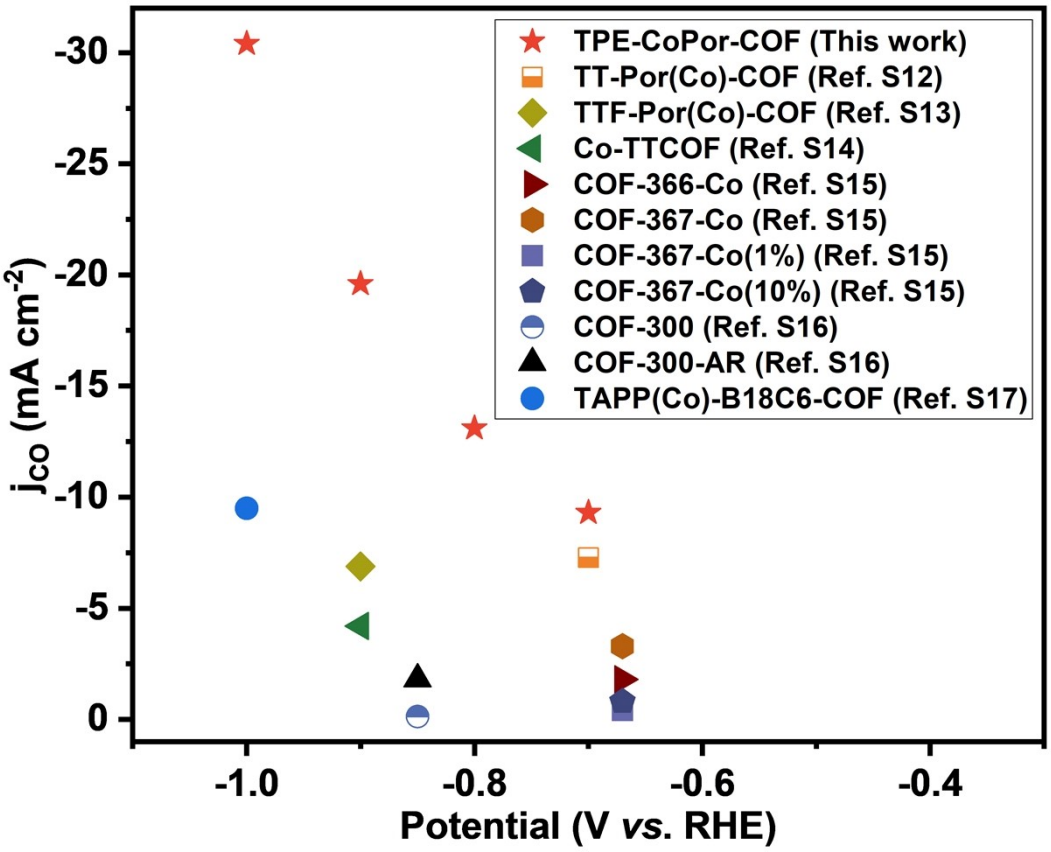

Fig. S23. Comparison of CO partial current density for CO_2 electroreduction.

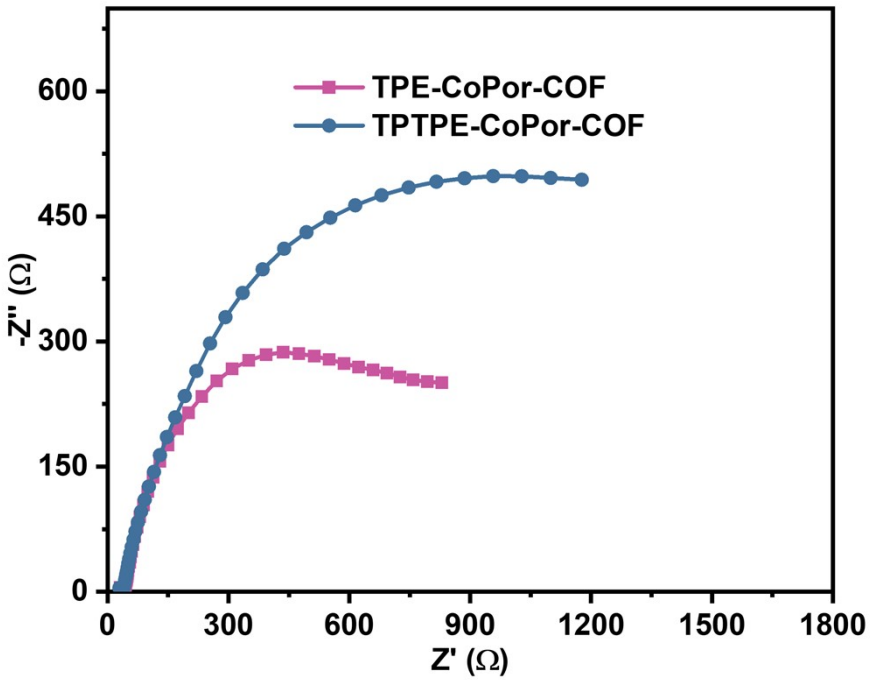

Fig. S24. EIS spectra of TPE-CoPor-COF and TPTPE-CoPor-COF.

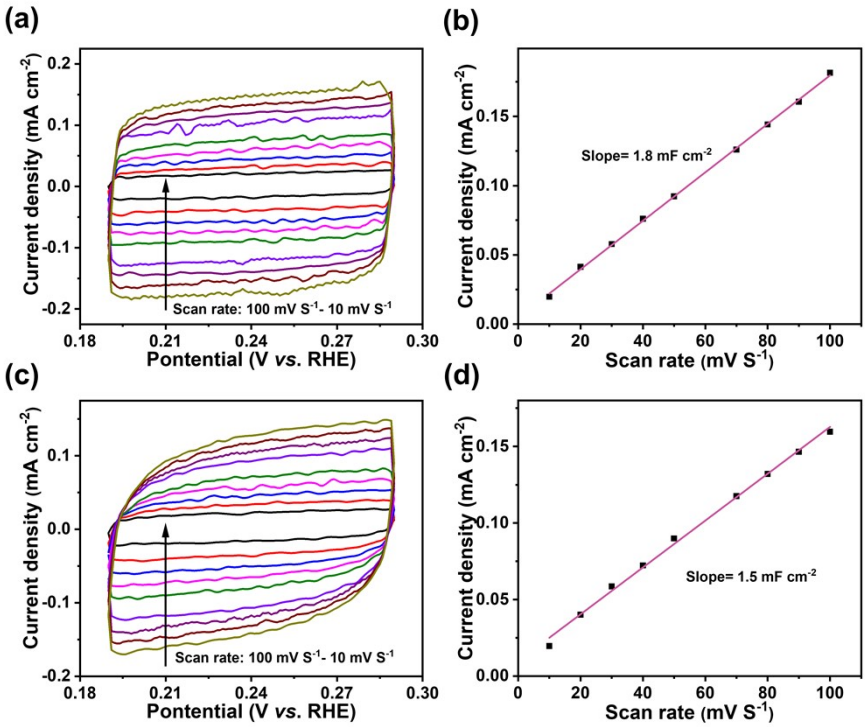

Fig. S25. Cyclic voltammogram (CV) curves in the region from 0.29 to 0.19 V *vs*. RHE at various scan rates (from 10 to 100 mV s^{-1}) and corresponding capacitive current at 0.05 V for TPE-CoPor-COF (a), (b) and TPTPE-CoPor-COF (c), (d).

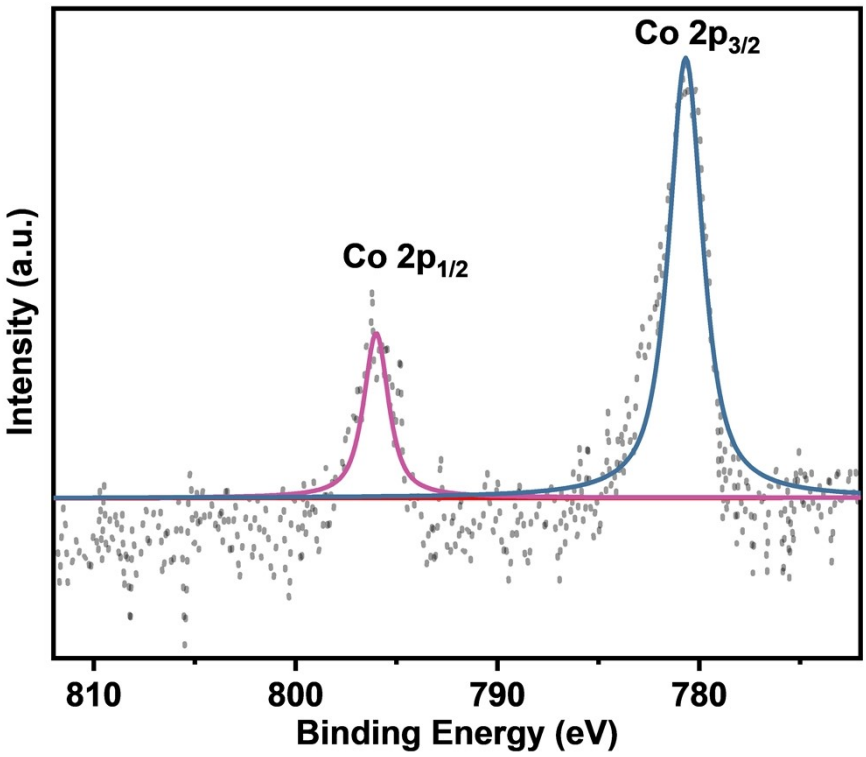

Fig. S26. High-resolution XPS scan of Co 2p for TPE-CoPor-COF after CO_2RR testing.

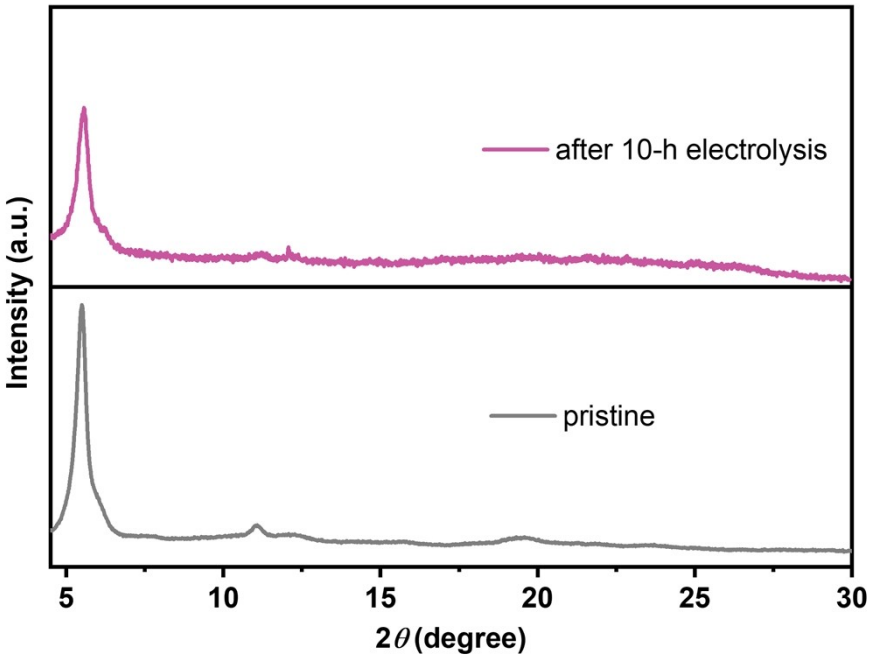

Fig. S27. PXRD patterns of TPE-CoPor-COF before and after CO_2RR testing.

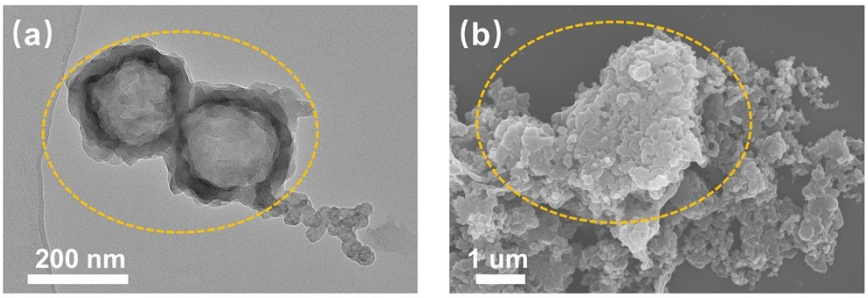

Fig. S28. TEM (a) and SEM (b) images of TPE-CoPor-COF after CO_2RR testing.

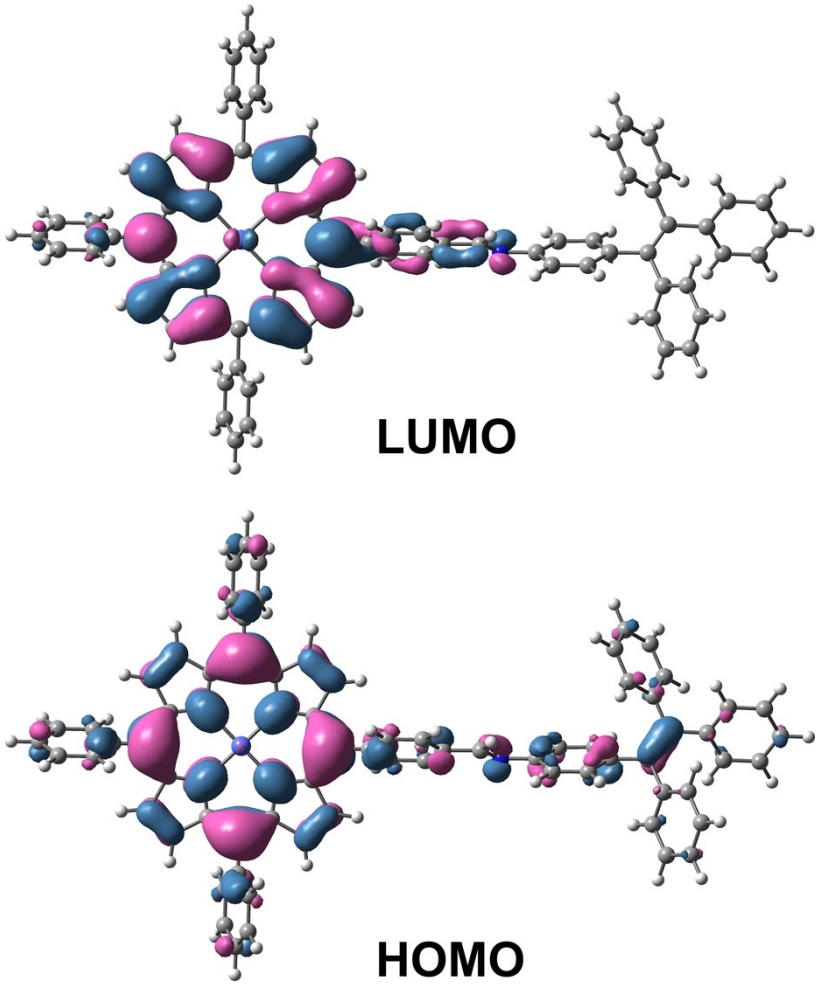

Fig. S29. The calculated LUMO and HOMO populations of the repeat unit in TPE-CoPor-COF (the isovalue of the surface is 0.02 a.u.).

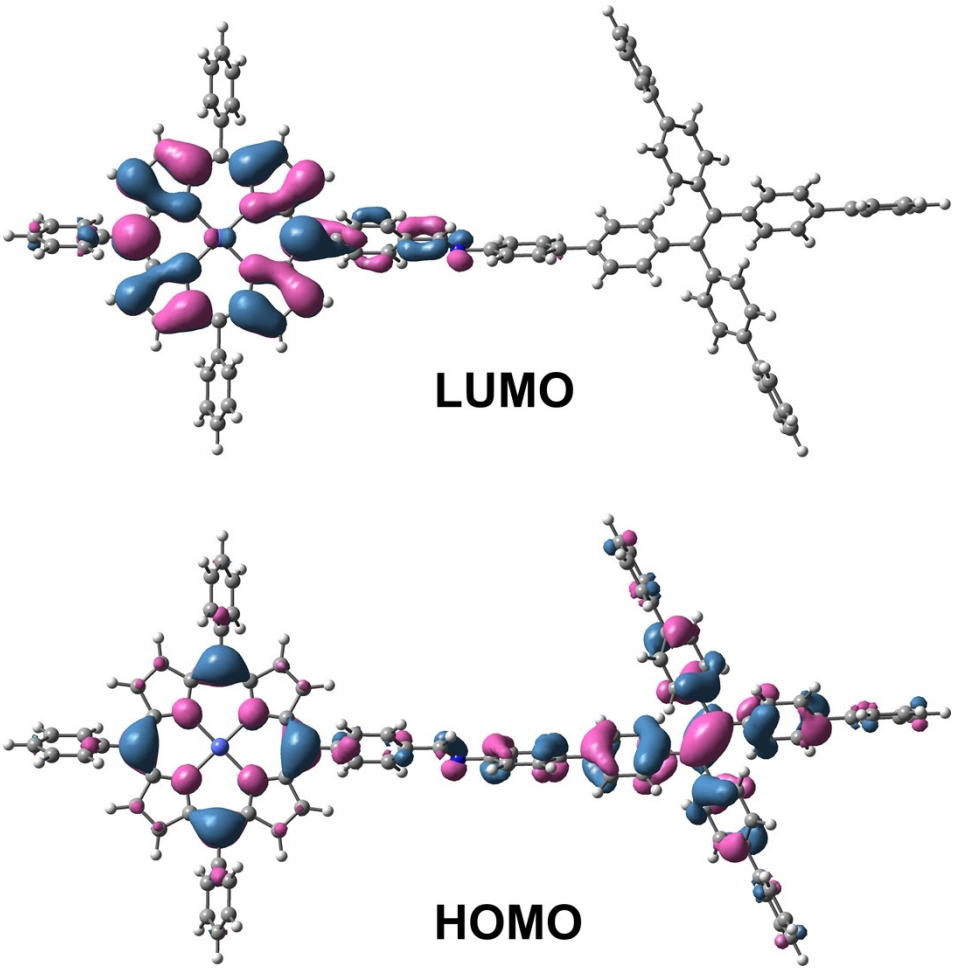

Fig. S30. The calculated LUMO and HOMO populations of the repeat unit in TPTPE-CoPor-COF (the isovalue of the surface is 0.02 a.u.).

Table S1. Fractional atomic coordinates in the refined unit cell of TPE-CoPor-COF.

Space group : *P*222 (TPE-CoPor-COF)							
a = 21.6952, b = 23.3738, c= 4.6216							
α = β = γ = 90º							
Atom	x	y	z	Atom	x	y	z
C1	0.18982	0.02895	2.00406	C18	0.43845	0.59075	1.76016
C2	0.11008	0.10397	2.00283	C19	0.43272	0.55293	1.98474
C3	0.1278	0.04683	2.00289	H20	0.22827	0.05779	2.01016
C4	0.03053	0.82119	2.00184	H21	0.06033	0.78427	2.00579
C5	0.04955	0.87984	1.99811	H22	0.13313	0.80645	1.62861
C6	0.15763	0.85121	2.01264	H23	0.19244	0.88248	2.40745
C7	0.16316	0.80753	1.81027	H24	0.21266	0.73289	1.6741
C8	0.19752	0.85062	2.24099	H25	0.27099	0.80892	2.45464
C9	0.20713	0.76525	1.83802	H26	0.31465	0.61889	2.3129
C10	0.24116	0.80802	2.27185	H27	0.40477	0.66492	1.54038
C11	0.24675	0.76473	2.06792	H28	0.38025	0.5348	2.35914
C12	0.29283	0.72026	2.09513	H29	0.47146	0.58175	1.59735
N13	0.31514	0.69438	1.87932	H30	0.30687	0.7098	2.32049
C14	0.35415	0.6477	1.92092	N31	0.08991	0	2
C15	0.34842	0.61045	2.15031	N32	0	0.91595	2
C16	0.39963	0.6369	1.72243	C33	0.46933	0.5	2
C17	0.38668	0.56364	2.18128	Ni34	0	0	0

Table S2. Fractional atomic coordinates in the refined unit cell of TPTPE-CoPor-COF.

Space group : *P*222 (TPTPE-CoPor-COF)							
a = 27.4053, b = 29.7918, c= 5.4579							
α = β = γ = 90º							
Atom	x	y	z	Atom	x	y	z
C1	0.14518	0.97658	1.00011	C23	0.31449	0.71606	0.70535
C2	0.08437	0.91584	1.00276	C24	0.29056	0.73185	0.91247
C3	0.09739	0.96218	1.00352	N25	0.25298	0.76191	0.87763
C4	0.02363	0.85499	0.99891	H26	0.05086	0.82642	0.99741
C5	0.03801	0.90248	0.99865	H27	0.17417	0.94977	0.99821
C6	0.12147	0.87979	1.01369	H28	0.11072	0.85388	0.64016
C7	0.13241	0.85168	0.81335	H29	0.13831	0.8953	1.39618
C8	0.14735	0.87423	1.22772	H30	0.17822	0.7988	0.65664
C9	0.16959	0.82088	0.82203	H31	0.20473	0.83886	1.41359
C10	0.18415	0.8432	1.23786	H32	0.25686	0.78421	1.23314
C11	0.1966	0.81681	1.03368	H33	0.48269	0.56915	0.65375
C12	0.23716	0.78674	1.05371	H34	0.40903	0.5264	1.31775
C13	0.449	0.54315	0.98638	H35	0.43457	0.64165	0.64043
C14	0.45533	0.57541	0.8002	H36	0.35928	0.59744	1.29418
C15	0.41471	0.55185	1.16272	H37	0.35051	0.66909	1.34343
C16	0.42852	0.61533	0.79097	H38	0.36851	0.6724	0.54953
C17	0.38738	0.59123	1.15149	H39	0.2873	0.72742	1.31251
C18	0.39376	0.62399	0.9652	H40	0.3044	0.73072	0.5204
C19	0.36218	0.66393	0.94766	N41	0.06792	0	1
C20	0.33992	0.68162	1.15494	N42	0	0.93187	1
C21	0.34966	0.6834	0.72244	Co43	0	0	1
C22	0.30488	0.71435	1.13995	C44	0.47634	0.5	1

Table S3. Metal contents of TPE-CoPor-COF and TPTPE-CoPor-COF calculated from ICP-OES tests.

Sample	Calculated (wt%)	Found (wt%)
TPE-CoPor-COF	5.34	3.94
TPTPE-CoPor-COF	4.18	4.15

Table S4. Comparison of the electrocatalytic performance for COF-based electrocatalysts in H-cells (0.5 M $KHCO_3$ aqueous solution).

Catalysts	Potential (V vs. RHE)	j_{CO} (mA cm^{-2})	FE_{CO} (%)	Ref
TPE-CoPor-COF	-1.0	-30.4	91	this work
	-0.9	-19.6	93	
	-0.8	-13.1	94	
	-0.7	-9.3	95	
TT-Por(Co)-COF	-0.7	-7.28	85	S12
TTF-Por(Co)-COF	-0.9	-6.88	78.5	S13
Co-TTCOF	-0.9	-4.2	59.5	S14
COF-366-Co	-0.67	-1.8	90	S15
COF-367-Co	-0.67	-3.3	91	
COF-367-Co(1%)	-0.67	-0.4	40	
COF-367-Co(10%)	-0.67	-0.8	70	
COF-300	-0.85	-0.13	53	S16
COF-300-AR	-0.85	-1.82	80	
TAPP(Co)-B18C6-COF	-1.0	-9.45	71.5	S17

REFERENCES

[1] R. Chen, Y. Wang, Y. Ma, A. Mal, X. Gao, L. Gao, L. Qiao, X. Li, L. Wu and C. Wang, *Nat. Commun.*, 2021, **12**, 1354.

[2] C. Adamo and V. Barone, *J. Chem. Phys.* 1999, **110**, 6158–6170.

[3] S. Grimme, S. Ehrlich and L. Goerigk, *J. Comput. Chem.* 2011, **32**, 1456–1465.

[4] D. Andrae, U. Häußermann, M. Dolg, H. Stoll and H. Preuß, *Theor. Chim. Acta* 1990, **77**, 123–141.

[5] P. C. Hariharan and J. A. Pople, *Theor. Chim. Acta* 1973, **28**, 213–222.

[6] M. S. Gordon, The Isomers of Silacyclopropane. *Chem. Phys. Lett.* 1980, **76**, 163–168.

[7] R. Binning and L. Curtiss, *J. Comput. Chem.* 1990, **11**, 1206–1216.

[8] M. J. Frisch, G. W. Trucks, H. B. Schlegel, G. E. Scuseria, M. A. Robb, J. R. Cheeseman, G. Scalmani, V. Barone, B. Mennucci, G. A. Petersson, H. Nakatsuji, M. Caricato, X. Li, H. P. Hratchian, A. F. Izmaylov, J. Bloino, G. Zheng, J. L. Sonnenberg, M. Hada, M. Ehara, K. Toyota, R. Fukuda, J. Hasegawa, M. Ishida, T. Nakajima, Y. Honda, O. Kitao, H. Nakai, T. Vreven, J. A. Montgomery, Jr., J. E. Peralta, F. Ogliaro, M. Bearpark, J. J. Heyd, E. Brothers, K. N. Kudin, V. N. Staroverov, T. Keith, R. Kobayashi, J. Normand, K. Raghavachari, A. Rendell, J. C. Burant, S. S. Iyengar, J. Tomasi, M. Cossi, N. Rega, J. M. Millam, M. Klene, J. E. Knox, J. B. Cross, V. Bakken, C. Adamo, J. Jaramillo, R. Gomperts, R. E. Stratmann, O. Yazyev, A. J. Austin, R. Cammi, C. Pomelli, J. W. Ochterski, R. L. Martin, K. Morokuma, V. G. Zakrzewski, G. A. Voth, P. Salvador, J. J.

Dannenberg, S. Dapprich, A. D. Daniels, O. Farkas, J. B. Foresman, J. V. Ortiz, J. Cioslowski, and D. J. Fox, Gaussian 09, Version D.01, Gaussian, Inc., Wallingford CT, 2013.

[9] A. V. Marenich, C. J. Cramer and D. G. Truhlar, *J. Phys. Chem. B*, 2009, **113**, 6378-6396.

[10] K. Chan and J. K. Nøskov, *J. Phys. Chem. Lett.* 2015, **6**, 2663–2668.

[11] A. A. Peterson, F. Abild-Pedersen, F. Studt, J. Rossmeisl, and J. K. Nøskov, *Energy Environ. Sci.* 2010, **3**, 1311–1315.

[12] Q. Wu, M. J. Mao, Q. J. Wu, J. Liang, Y. B. Huang and R. Cao, *Small*, 2021, **17**, 2004933.

[13] Q. Wu, R. Xie, M. Mao, G. Chai, J. Yi, S. Zhao, Y. Huang and R. Cao, *ACS Energy Lett.*, 2020, **5**, 1005-1012.

[14] H. Zhu, M. Lu, Y. Wang, S. Yao, M. Zhang, Y. Kan, J. Liu, Y. Chen, S. Li and Y. Lan, *Nat. Commun.*, 2020, **11**, 497.

[15] S. Lin, C. S. Diercks, Y. B. Zhang, N. Kornienko, E. M. Nichols, Y. Zhao, A. R. Paris, D. Kim, P. Yang, O. M. Yaghi and C. J. Chang, *Science*, 2015, **349**, 1208-1213.

[16] H. Liu, J. Chu, Z. Yin, X. Cai, L. Zhuang and H. Deng, *Chem*, 2018, **4**, 1696-1709.

[17] S. An, C. Lu, Q. Xu, C. Lian, C. Peng, J. Hu, X. Zhuang and H. Liu, *ACS Energy Lett.*, 2021, **6**, 3496-3502.